Journal of
Synchrotron
Radiation

ISSN 0909-0495

Received 23 July 2010
Accepted 25 August 2010

Design and construction of a compact end-station at NSRRC for circular-dichroism spectra in the vacuum-ultraviolet region

Szu-Heng Liu, Yi-Hung Lin, Liang-Jen Huang, Shiang-Wen Luo, Wan-Lin Tsai, Su-Yu Chiang and Hok-Sum Fung*

National Synchrotron Radiation Research Center, 101 Hsin-Ann Road, Hsinchu Science Park, Hsinchu 30076, Taiwan. E-mail: hsfung@nsrrc.org.tw

A synchrotron-radiation-based circular-dichroism end-station has been implemented at beamline BL04B at the National Synchrotron Radiation Research Center (NSRRC) in Taiwan for biological research. The design and performance of this compact end-station for measuring circular-dichroism spectra in the vacuum-ultraviolet region are described. The linearly polarized light from the beamline is converted to modulated circularly polarized light with a LiF photoelastic modulator to provide a usable wavelength region of 130–330 nm. The light spot at the sample position is 5 mm × 5 mm at a slit width of 300 μm and provides a flux greater than 1×10^{11} photons s^{-1} (0.1% bandwidth)$^{-1}$. A vacuum-compatible cell made of two CaF_2 windows has a variable path length from 1.3 μm to 1 mm and a temperature range of 253–363 K. Measured CD spectra of (1*S*)-(+)-10-camphorsulfonic acid and proteins demonstrated the ability of this system to extend the wavelength down to 172 nm in aqueous solution and 153 nm in hexafluoro-2-propanol.

Keywords: synchrotron radiation circular dichroism; photoelastic modulator; vacuum-ultraviolet region; camphorsulfonic acid; protein secondary structure.

1. Introduction

A circular-dichroism (CD) spectrum measures the difference in the absorption of left-handed *versus* right-handed circularly polarized light by chiral molecules. It is widely used to provide structural information about biopolymers such as proteins, nucleic acids and sugars in solution, hence complementing information from X-ray crystallography (Majava *et al.*, 2008), small-angle X-ray scattering (Grossmann *et al.*, 2002; Stanley *et al.*, 2004) and NMR spectra (Watkins *et al.*, 2008). Proteins with varied secondary structures such as α-helix, β-strand and random coil have distinctive CD spectra (Wallace & Janes, 2001). Previous authors have used CD spectra to monitor the variation of secondary structures of components of aqueous proteins under thermal, pH and ionic stresses (Toumadje & Johnson, 1995; Durell *et al.*, 1988; Hennessey *et al.*, 1987). CD has also been applied to determine whether protein–protein or protein–ligand interactions alter the conformation of a protein, and demonstrate its potential in biomedical applications such as the intensive screening of drugs (Wallace & Janes, 2003).

Before the development of the photoelastic modulator (PEM) (Kemp, 1969) the main experimental scheme employed in recording CD required separate measurements of the absorption of left and right circularly polarized light followed by subtraction. For the vacuum-ultraviolet (VUV) region, a static quarter-wave retarder, a MgF_2 or sapphire birefringent crystal, a stressed LiF plate or a MgF_2 or LiF Fresnel rhomb generated the left and right circularly polarized light separately. The first reported CD measurement in the VUV region (Feinleib & Bovey, 1968) was made on *S*-(+)-3-methylcyclopentanone (I); separate photomultiplier tubes measured the absorption of left and right circularly polarized light, and subtraction was effected using a d.c. bridge circuit.

In order to measure CD, in 1969 Kemp introduced the PEM, a birefringent crystal bar modulator with an acoustic wave and driven with a piezoelectric transducer. When linearly polarized light passes a birefringent crystal bar with its axis at 45°, the PEM converts it to left and right periodically circularly polarized light. Because a PEM can generate modulated circularly polarized light at a fixed frequency, a lock-in amplifier, a box-car integrator or a high-speed analogue-to-digital converter (Khazimullin & Lebedev, 2010) serves to measure the circular-absorption signal with great sensitivity. For this reason the PEM has become mainstream for measurement of vacuum-ultraviolet circular dichroism (VUVCD) (Schnepp *et al.*, 1970; Johnson, 1971; Pysh, 1976; Drake & Mason, 1977). The history of the development of VUVCD is presented elsewhere (Drake & Mason, 1978, and references therein).

Table 1
Specifications of principal optical components on beamline BL04B SNM.

	Deflection mirror M1	Pre-focusing mirror M2	Pre-focusing mirror M3	Entrance slit S1 Exit slit S2	Grating G	Refocusing mirror M4
r_1; r_2 (mm)	6100; ∞	6200; 6200 (V), 6535 (H)	335; 70		818; 818	70; 800
Deviation angle (2θ)	140°	140°	125.125°		70.25°	125.125°
	Plane	Toroid	Circular, cylinder	Bilaterally adjustable	Sphere	Circular, cylinder
Dimensions, L × W × H (mm)	150 × 100 × 25	150 × 100 × 25	20 × 20 × 10	H: 4 (fixed size), V: 5–3000 µm	50 × 30 × 20	20 × 20 × 10
Coating	SiC	SiC	SiC		Al + MgF_2/Au/Pt	SiC
Substrate	CVD-SiC	CVD-SiC	CVD-SiC	Stainless steel S-410	Borosilicate glass	CVD-SiC
Curvature (mm)	∞	Tangential: 18130; sagittal: 2160	251		1000	279
Ruling density (grooves mm^{-1})					600/1200/2400	

Synchrotron-based CD end-stations appeared after 1980 (Snyder & Rowe, 1980). Relative to a xenon arc lamp as a source in conventional instruments, a synchrotron is an ideal source of photons for VUVCD experiments by virtue of its great flux, well defined polarization and continuous spectrum. This source offers significant improvements for CD measurements over the VUV region, <190 nm. The superior flux improves the signal-to-noise ratio of a spectrum, such that a spectrum of a protein in aqueous solution might be recorded accurately to ~160 nm; the limit for a xenon arc lamp is at best ~185 nm (Wallace, 2000). In the case of water removal, such as for a partially hydrated sample, or a sample dissolved in a slightly absorbing organic solvent such as hexafluoro-2-propanol (HFIP), a spectrum of a protein is measurable to ~140 nm, so that a CD signal originating from energetic transitions can be captured (Clarke & Jones, 2004). Several authors have demonstrated the benefits of CD with synchrotron radiation (SRCD) relative to conventional CD for saccharides (Gekko & Matsuo, 2006), glycosaminoglycans (Matsuo *et al.*, 2009) and membrane proteins in lipid systems (Miles *et al.*, 2008*a*). The modern techniques and applications for SRCD are presented by Wallace & Janes (2009).

In the present work we have developed a compact VUVCD end-station at beamline BL04B at NSRRC in Taiwan for biological research, such as structural investigation of biopolymers in solution and protein folding dynamics. The design and performance are discussed in the following sections.

2. Apparatus

2.1. BL04B Seya-Namioka (SNM) beamline

The layout of the BL04B SNM beamline (Tseng *et al.*, 1995) is shown in Fig. 1; the specifications of the principal optical components are listed in Table 1. This beamline provides VUV light from 50 to 400 nm. The horizontal angular acceptance is 14 mrad. The vertical angular acceptance is variable from 2 to 6 mrad and is controlled by a pair of motorized baffles. When the widths of the entrance and exit slits are both 300 µm the wavelength resolution is about 0.5 nm (with a grating having 600 grooves mm^{-1}). The wavelength accuracy is ±0.2 nm, calibrated with Mg and Ca vapour absorption for the spectral range 160–290 nm. The flux exceeds 1×10^{11} photons s^{-1} (0.1% bandwidth)$^{-1}$ at a 300 mA ring current. The area of the focal spot is 1.3 mm (H) × 0.8 mm (V).

2.2. VUVCD end-station

The layout of the VUVCD end-station is shown in Fig. 2. This end-station comprises four principal parts: a port for differential pumping, a chamber for a PEM, a sample chamber and a photomultiplier tube (PMT) as detector; these parts are connected with O-ring (Viton) sealed rotatable hollow tubes. This design allows free rotation of the PEM chamber and the PMT along the axis of the light path under vacuum. The differential pumping port, directly connected to beamline BL04B, is pumped with a turbomolecular pump (400 L s^{-1}) to a base pressure of 2×10^{-9} torr without baking. The PEM chamber is equipped with an ultrahigh-vacuum-type PEM (Hinds LF 50) and is pumped with a turbomolecular pump (70 L s^{-1}) to a base pressure of 5×10^{-9} torr. This vacuum is sufficient such that an isolating window is unnecessary between the PEM chamber and the differential pumping port.

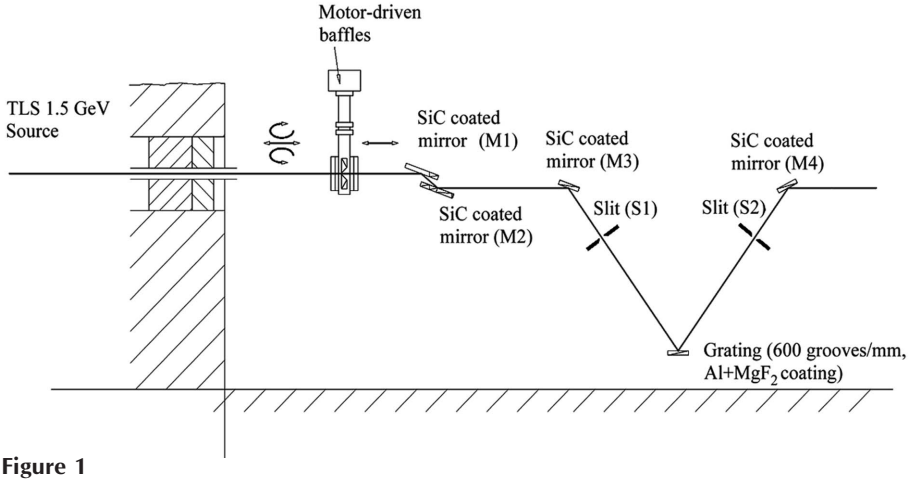

Figure 1
Optical layout of beamline BL04B SNM at NSRRC.

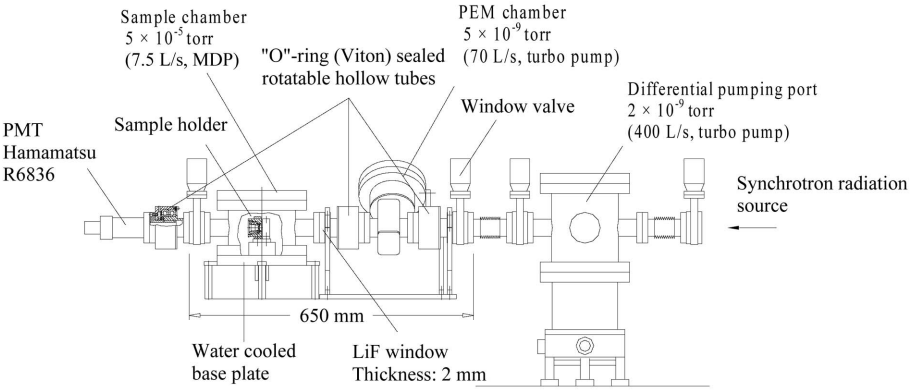

Figure 2
Set-up of the VUVCD end-station.

A hollow tube rotatable under vacuum is connected to each port, entrance and exit, of the PEM chamber; this design allows free rotation of the PEM chamber along the light path. The PEM LiF crystal bar is oriented at 45° relative to the direction of linear polarization of the incident light.

The sample chamber (stainless steel) is pumped with a molecular drag pump (Drytel 31, Alcatel); the ultimate pressure attains 5×10^{-5} torr, monitored with a wide-range gauge (WRG, BOC Edwards). The system is pumped from atmospheric pressure to 5×10^{-5} torr within 15 min. A window (LiF, thickness 2 mm, diameter 25 mm) is placed between the sample chamber and the PEM chamber in order to maintain the pressure of the PEM chamber at 5×10^{-9} torr, when the sample chamber is vented to the atmosphere. A PMT (solar-blind, R6836, Hamamatsu) is connected to the sample chamber with a rotatable hollow tube; the PMT is sealed with this tube by an O-ring (Viton).

A block (copper, internally cooled with water) is blazed to the base plate of the sample chamber. The sample holder is fixed to the copper block with a clamp. A Peltier thermoelectric unit (T-E, two stages) is installed between the sample holder and the copper block. This unit can heat or cool the sample holder through application of a controlled polarity of bias. The temperature range of the sample holder thus achieved is 253–363 K.

A schematic drawing of the sample holder is shown in Fig. 3; the holder is made of copper plated with nickel to avoid corrosion from chemical compounds. The sample cell has two windows (CaF_2, 'D'-shape, thickness 2 mm, UV grade; International Crystal Laboratories, Garfield, NJ, USA); the shape of these windows matches the 'D'-shape of a groove in the sample holder. This design enables the orientation of the windows to be fixed during sample loading and installation of the windows. Three O-rings (Viton) seal the windows with the sample holder. The length of the optical path is controlled by means of a spacer with variable thickness from 1.3 µm (without spacer) to 1 mm. Two types of donut-shaped spacers are used for the sample cell, one is made of Kapton and the other of Teflon. The thicknesses of the Kapton spacers are 7 µm, 25 µm, 50 µm and 125 µm; the thicknesses of the Teflon spacers are 0.5 mm and 1 mm. The maximum diameter of the clear aperture of the sample cell is 13 mm. The area of the beam spot at the sample position is 5 mm × 5 mm (H × V, FWHM).

2.3. Data acquisition system

A flow chart of the system for data acquisition is shown in Fig. 4. The PEM (LF50) and the SNM wavelength setting are controlled with a computer through an interface (RS232). The PMT measures the transmitted intensity of the light. The PMT signal is amplified with a preamplifier (C7319, Hamamatsu) with gain factor 10^6 V A^{-1} and bandwidth 200 kHz. The preamplifier output, V_{PMT}, feeds into the PMT HT servo (Aviv Biomedical) and the unit for signal conditioning (SCU100, Hinds). The servo maintains V_{PMT} at 1 V with variation less than 0.5% during wavelength scanning. The signal-conditioning unit separates the V_{PMT} into a.c. ($V_{a.c.}$) and d.c. ($V_{d.c.}$) signals. The PEM controller (Hinds 100) provides a reference signal for the lock-in amplifier (Signal Recovery 5210) to measure $V_{a.c.}$. The DAQ (16 bit, NI USB-6229, National Instruments) monitors $V_{lock\text{-}in}$ and $V_{d.c.}$. The CD signal is proportional to the ratio $V_{lock\text{-}in}/V_{d.c.}$.

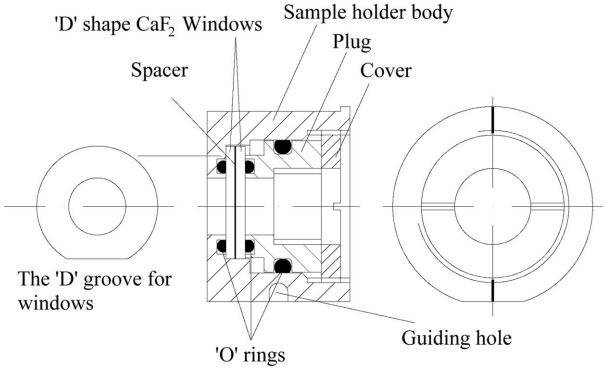

Figure 3
Structure of the VUVCD sample holder.

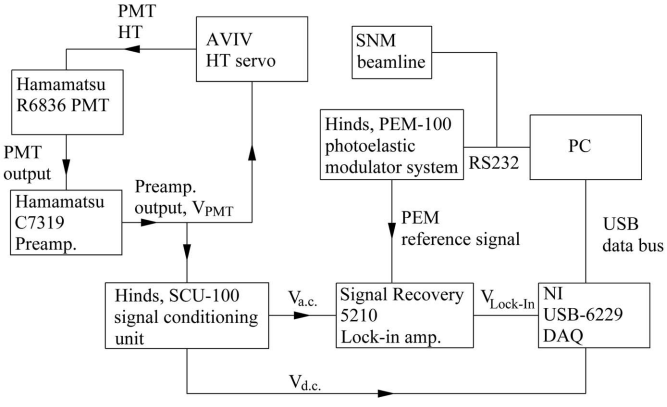

Figure 4
System for data acquisition at the VUVCD end-station.

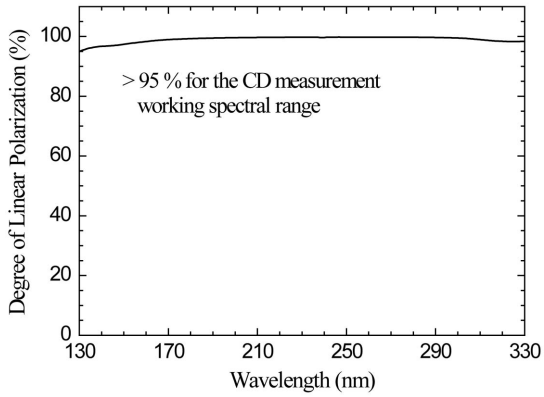

Figure 5
Measurement of the degree of linear polarization at beamline BL04B SNM.

3. System performance

3.1. Polarization of synchrotron light at beamline BL04B

To measure the source polarization we use a prism (MgF_2, Rochon type, MFRV9, Karl Lambrecht) to separate the *s*- and *p*-polarization rays; the angular separation is 4.6–5.4° for the *s*- and *p*-polarization rays in the region 140–546 nm. The degree of linear polarization is defined by $D = |I_p - I_s|/(I_p + I_s)$, where I_p and I_s represent the intensities of the *p*- and *s*-polarization. The angle of the prism for measuring I_s is optimized at 200 nm by maximizing the on-axis intensity, and the angle for measuring I_p is obtained by minimizing the on-axis intensity. Fig. 5 shows the measured degree of linear polarization, which is more than 95–98% in the region 130–330 nm. Our value is compatible with that of CD12 SRCD (Clarke & Jones, 2004) and is suitable for the measurement of CD spectra.

3.2. Performance of the PEM system and the effect of optical birefringence

With a birefringent optical element, the PEM can generate modulated circularly and linearly polarized light. In our work the monochromatic and linearly polarized radiation from the synchrotron passes the LiF crystal (LF50 PEM) at 45° to the bar axis. The PEM is controlled at a 50 kHz resonance; it converts linearly polarized light to left and right periodically circularly polarized light at 50 kHz.

A method of oscilloscope calibration (described in the Hinds PEM-100 operation manual, Hinds Instruments) is used to test the performance of the PEM system. According to this method, a prism (MgF_2, Rochon) that serves as an analyzer is placed between the PEM and the PMT. The prism is set orthogonal with linearly polarized light; accordingly, if the PEM is turned off, the PMT output signal tends to zero. Using the PEM-100 factory-default working curve ($\lambda/2$ retardation) to drive the LF50 PEM and adjusting the PEM orientation to maximize the observed PEM-modulated output light signal, a signal (100 kHz) shows on the oscilloscope. We tested signal patterns at wavelengths of 160 and 240 nm. When the factory-default working curve is used, the maximum oscillating signal patterns are observed.

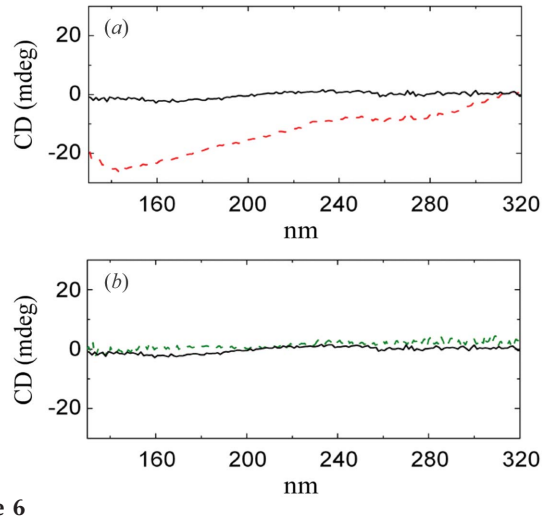

Figure 6
(*a*) VUVCD baselines measured under vacuum without a CaF_2 cell at the end-station. Red dashed line: CD baseline before orientation of the PMT to the optimum angle. Black solid line: PMT oriented to the optimum angle. The baseline amplitude is as small as ±2 mdeg for the spectral range 130–320 nm. (*b*) Baseline spectra acquired without (black solid line) and with (green dashed line) the CaF_2 sample cell. All spectra were recorded with slit width 300 µm, single scan, time constant 1 s and wavelength increments 0.6 nm.

The residual birefringence of optical elements, *i.e.* PEM crystal, LiF window and the PMT window, in the system affects the baseline of the CD spectrum. It is thus essential to minimize the effect to obtain a smooth and small background. Fig. 6(*a*) shows the CD signals in the 130–320 nm region with only the PEM, LiF window and PMT working. Without an optimization of the orientation of the PMT, a negative band was observed at ∼144 nm (shown by the red dashed line). With the photon wavelength and PEM set at 144 nm, we rotate the PMT to allow the CD signal to tend to zero; the rescanned CD spectrum is shown by a black solid line. The system CD baseline is down to ±2 mdeg and the deviation about ±0.2 mdeg. Furthermore, the optical elements can compensate one another to decrease the residual birefringence of the system based on Fukazawa's concept (Fukazawa & Fujita, 1996). For each CaF_2 sample cell, we measured the CD spectrum of each cell window and found a pair of windows to compensate each other. In this system the CD baseline is controlled within ±2.5 mdeg and its deviation about ±0.3 mdeg for the spectral range (Fig. 6*b*).

4. CD test measurements

4.1. Materials and sample preparation

Deuterium oxide (99.9 at.% D), HFIP, (1*S*)-(+)-10-camphorsulfonic acid (CSA), myoglobin (≥95%), concanavalin A from Jack bean (type IV), bovine serum albumin (BSA) (≥96%) and human serum albumin (HSA) (≥97%) were purchased (Sigma-Aldrich, St Louis, MO, USA). Before CD measurements, protein solutions were centrifuged at 20000*g* for 5 min to remove the aggregates. Protein concen-

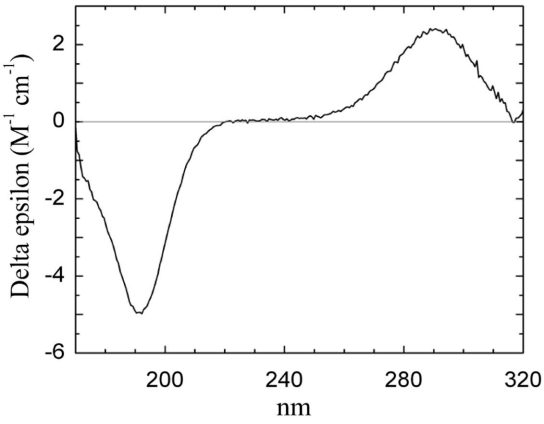

Figure 7
Spectrum of CSA aqueous solution (H_2O baseline subtracted) recorded at the BL04B (SNM) VUVCD end-station. CD signals were collected with time constant 1 s and wavelength increments 0.6 nm at 298 K. The plot is an average of five measurements. Characteristic signals are observed at 192.5 ($\Delta\varepsilon$ = −4.87) and 290 nm ($\Delta\varepsilon$ = +2.41). The ratio of signals at 192.5 and 290 nm is 2.02.

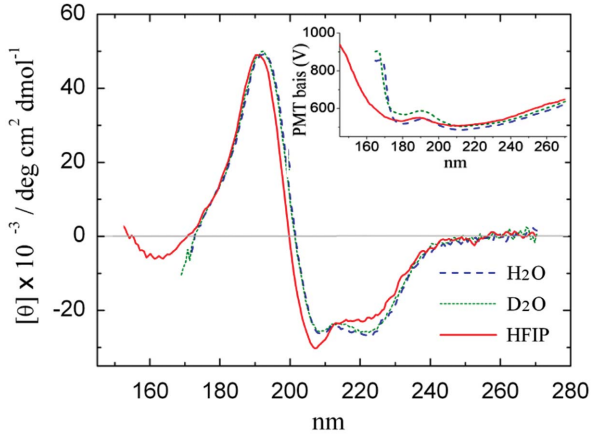

Figure 8
Spectra of myoglobin dissolved in H_2O, D_2O and HFIP at 298 K (solvent baseline subtracted, triplicate scans averaged). The spectra were recorded with a CaF_2 cell (path length 7 µm), wavelength increment 0.6 nm and time constants 1 s for a sample in D_2O and H_2O or 10 s for its counterpart in HFIP. The inset shows the voltage of the PMT recorded for each sample over the measured range of wavelength.

trations were determined using the method of Bradford (1976).

4.2. Calibration of the VUVCD end-station

CSA is a standard substance commonly used to calibrate the wavelength and ellipticity of CD instruments (Chen & Yang, 1977). We used a two-point calibration method with CSA to test the performance of the BL04B (SNM) VUVCD end-station. CSA of more than 98% was purchased from Sigma-Aldrich and the concentration of aqueous CSA was estimated at $A_{285\,nm}$ as reported (Miles *et al.*, 2004). Fig. 7 shows the spectrum of CSA in the 172–320 nm region that agrees satisfactorily with that reported from other SRCD systems (Clarke & Jones, 2004; Johnson, 1996). The ratio of the signals at 192.5 and 290 nm was 2.02, exactly as expected (Miles *et al.*, 2003).

4.3. VUVCD spectra of proteins

We examined the spectra of α-helix-rich protein myoglobin in H_2O, D_2O and HFIP at a concentration of 10 mg ml^{-1} (Fig. 8); the path length is 7 µm in the measurement. The myoglobin CD spectrum was measurable to ∼172 nm in H_2O, ∼168 nm in D_2O but ∼153 nm in HFIP; below these wavelengths the CD signal became unreliable owing to the high absorbance of solvents. In Fig. 8 the CD spectra of myoglobin in H_2O and D_2O are similar over a wavelength range of 172–270 nm. The spectra recorded in HFIP differed significantly from those in H_2O and D_2O because of the variation of the protein conformation dependent on the organic solvent. Accordingly, the ratio between CD signals at 208 and 222 nm altered, and the CD maximum about 192 nm shifted to ∼190 nm. Our results agree satisfactorily with those of CD12 SRCD (Clarke & Jones, 2004).

Fig. 9(*a*) shows typical spectra of three standard proteins in H_2O. SDS-PAGE analysis indicated that the purity of the proteins used in this study was sufficiently high for CD measurements (Fig. 9*b*). α-Helix-rich proteins myoglobin and bovine serum albumin (BSA) exhibit one positive signal at ∼192 nm, originating from the π–π^* perpendicular transition, and two negative signals at ∼208 and 222 nm, originating from the π–π^* parallel and n–π^* transitions, respectively. The β-strand-rich protein concanavalin A exhibits a positive feature at ∼198 nm, originating from the π–π^* transition, and a negative feature at ∼225 nm, originating from the n–π^* transition. These spectra agree satisfactorily with those published previously (Gekko *et al.*, 2005; Clarke & Jones, 2004). To further understand the relation between the CD signals and sample concentration, Fig. 9(*c*) shows the CD signals of these three standard proteins as a function of concentration. It is clear that the magnitude of CD originating from various electronic transitions increased linearly with increasing concentration of protein (myoglobin and BSA, 0.6–25 mg ml^{-1}; concanavalin A, 0.6–20 mg ml^{-1}; path length 7 µm). As the protein concentration became too great, because of the large PMT bias, the major features about 192 nm (myoglobin and BSA) and 198 nm (concanavalin A) become inaccurately recorded as having smaller magnitudes (Fig. 9*c*, labelled filled down triangles).

4.4. Dynamic range of the CD spectrum

To decrease the wavelength of the limit for aqueous protein spectra, a short path length is essential to decrease the water absorption (Wallace *et al.*, 2004). However, for a protein sample with a small concentration and short path length, the range of the CD spectrum might be only a few millidegrees. To examine the performance of the 'weak-signal' measurements, we recorded spectra with the H_2O baseline subtracted of aqueous myoglobin (0.57 and 1.15 mg ml^{-1}) in a CaF_2 cell (path length 7 µm). Even when the magnitude was small, the spectra were detectable and showed a linear dependence on concentration (Fig. 10, comparison of two spectra). We then estimated the content of protein secondary structure with a

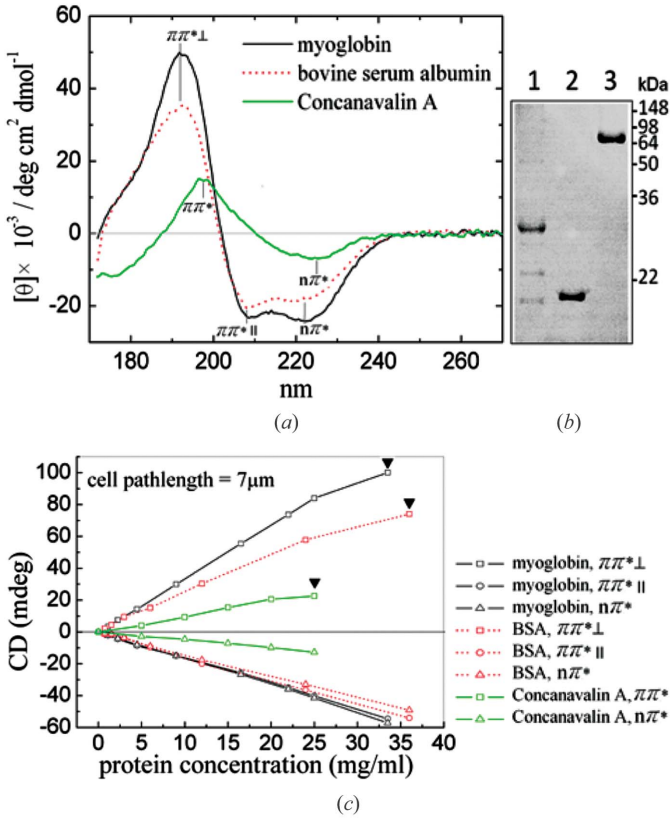

Figure 9
Spectra of standard proteins in aqueous solution (H_2O baseline subtracted, triplicate scans averaged). (*a*) Spectra from α-helix-rich proteins myoglobin, BSA and β-strand-rich protein concanavalin A, in mean residue ellipticity units. (*b*) SDS-PAGE analysis of proteins for CD measurements. Concanavalin A (1 µg in lane 1), myoglobin (1 µg in lane 2) and BSA (1.5 µg in lane 3) were separated using a 12.5% SDS-gel. Proteins in the resultant gel were stained with Coomassie blue. (*c*) CD spectra; linear dependence on concentration of these three standard proteins. Each magnitude of the CD signal for various electronic transitions exhibits a linear relation with protein concentration. Filled down triangles: data points under mis-recorded condition caused by excessive concentration of protein. Symbols of electronic transition: π–π* perpendicular ($\pi\pi^*\perp$); π–π* parallel ($\pi\pi^*\|$); π–π* ($\pi\pi^*$); n–π* ($n\pi^*$). All spectra were recorded with varied combination of protein concentration in a CaF_2 cell (path length 7 µm), time constant 1 s and wavelength increment 0.6 nm at 298 K.

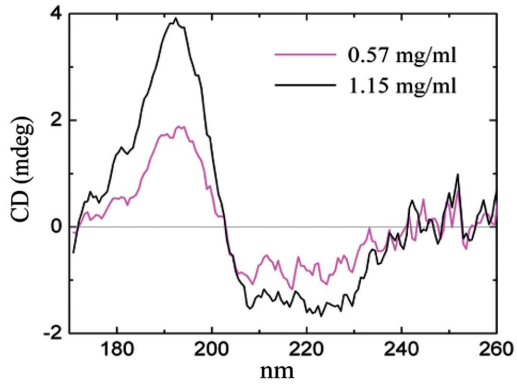

	Secondary Structure (%)		
	α- Helix	β-Strand	Turn
Reported (Matsuo et al., 2004)	75.8	0	12.4
Protein Concentration (mg/ml)			
16.5	75	0	10
4.5	76	4	8
2.25	75	6	7
1.15	67	9	9
0.57	69	11	10

Figure 10
Detection limit of the BL04B (SNM) VUVCD end-station. All spectra were recorded with slit width 300 µm, time constant 10 s, single scan and without smoothing. Upper panel: spectra of aqueous myoglobin (0.57 and 1.15 mg ml^{-1}) in a CaF_2 cell (path length 7 µm, H_2O baseline subtracted), representing samples with a 'weak signal'. Lower table: results of online analysis (DichroWeb) of protein secondary structure calculated from spectra of myoglobin at weak signals (0.57 and 1.15 mg ml^{-1}) and signals from regular concentrations (2.25 mg ml^{-1}, 4.5 mg ml^{-1} and 16.5 mg ml^{-1}).

weak signal (myoglobin 0.57 mg ml^{-1}) using an online server (DichroWeb, http://dichroweb.cryst.bbk.ac.uk/; Whitmore & Wallace, 2008) with the CDSSTR algorithms and SP175 reference dataset (Fig. 10, lower table). The predicted α-helix content is ~69% in total, which agrees satisfactorily with a prediction from a counterpart at a 29-fold concentration (16.5 mg ml^{-1}, ~75%) and the standard value reported in the literature (~76%) (Matsuo *et al.*, 2004). There are more characteristics of strand-like structure (~11% in total), which might be due to the spectral shape of the weak signal being noisy; the noise contributes to the apparent characteristics of the spectra. These results indicate that, even when the magnitude is small, the spectra remain within acceptable levels for predicting the secondary structure of a protein for this sample. Hence, together with Fig. 9, we conclude that the instruments at the BL04B (SNM) VUVCD end-station are able to measure the CD signal from a few to as many as 80–90 millidegrees.

4.5. Radiation damage

The damage to a protein induced by synchrotron radiation depends on the density of photon flux at the sample (Miles *et al.*, 2008*b*). The effect of this signal deterioration is significant when scans are obtained at beamlines with a large flux density (>10^{12} photons s^{-1} mm^{-2}; Wien *et al.*, 2005). For a general-purpose SRCD beamline, the maximum flux density at the sample should be 4 × 10^{10} photons s^{-1} mm^{-2} (Miles *et al.*, 2008*b*). The radiation damage to a protein sample is expected to be negligible at our end-station on BL04B because the flux at the sample is 1 × 10^{11} photons s^{-1} (0.1% bandwidth)$^{-1}$ at a ring current of 300 mA, and the spot size is 5 mm (H) × 5 mm (V) (FWHM). The light flux density is thus 0.4 × 10^{10} photons s^{-1} mm^{-2}. To verify this expectation, CD spectra of the same HSA sample were scanned in a series from 175 to 270 nm, recorded at 14 min intervals (Fig. 11*a*); spectra were recorded with a CaF_2 cell (path length 7 µm), time constant 3 s, wavelength increment 0.6 nm and at 298 K. The spectra exhibited no alteration after the sample was maintained under radiation for at least 84 min [Fig. 11(*b*), black solid line]. After a protracted measurement (560 min), the CD signal in the

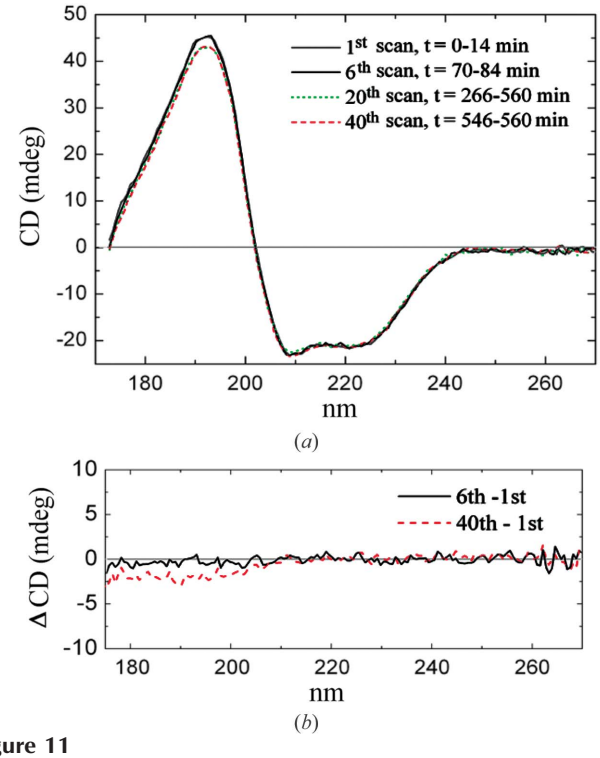

Figure 11
Radiation damage of a protein sample is negligible at the BL04B (SNM) VUVCD end-station. (*a*) HSA (Sigma-Aldrich) in H_2O (concentration 12 mg ml^{-1}). Spectra of the same aqueous sample in series were scanned from 175 to 270 nm and recorded at 14 min intervals. For clarity, only spectra of the 1st, 6th, 20th and 40th scans are shown. (*b*) Difference between scans over the wavelength range 175–270 nm. Black solid line: 6th–1st; red dashed line: 40th–1st.

region below 200 nm exhibited only a slightly decreased magnitude (∼5%) [Fig. 11(*b*), red dashed line]. These results indicate that the effects of radiation damage for the end-station at BL04B are insignificant.

5. Summary

We constructed a compact VUVCD end-station at the National Synchrotron Radiation Research Center, Taiwan. Optimizations of the performance of this end-station connected to beamline BL04B were undertaken with the following results. The flux of this beamline is suitable for measurements on protein samples; the effects of thermal denaturation induced by radiation on protein samples were slight. For the calibration of ellipticity magnitude and wavelength, the CD spectra of CSA in the region 170–320 nm agree satisfactorily with those properties measured at other operational SRCD systems. Demountable CaF_2 cells with optimized pairing are capable of measuring the CD spectra of myoglobin to 172 nm in H_2O, to 168 nm in D_2O and to 153 nm in HFIP. When the magnitude was as small as a few millidegrees, the spectra were clearly detectable and found to be within acceptable levels of an 'ideal spectrum' for this sample. A unit for temperature control was constructed at this end-station such that the dependence of CD spectra on temperature is measurable from 253 to 363 K.

We thank Professor B. A. Wallace (Birkbeck College, University of London, UK) and Dr R. W. Janes (Queen Mary College, University of London, UK) for their encouragement and helpful suggestions, Dr Lou-Sing Kan (Institute of Chemistry, Academia Sinica, Taiwan) for kind assistance in the design of the sample chamber, and Dr Yi-Cheng Chen (Mackay Medical College, Taiwan) and Dr Chien-I Ma (NSRRC, Taiwan) for critical reading of the manuscript.

References

Bradford, M. M. (1976). *Anal. Biochem.* **72**, 248–254.
Chen, G. C. & Yang, J. T. (1977). *Anal. Lett.* **10**, 1195–1207.
Clarke, D. T. & Jones, G. (2004). *J. Synchrotron Rad.* **11**, 142–149.
Drake, A. & Mason, S. F. (1977). *Tetrahedron*, **33**, 937–949.
Drake, A. F. & Mason, S. F. (1978). *J. Phys. Colloq.* **39**, C4-212–C4-220.
Durell, S. R., Gross, E. L. & Draheim, J. E. (1988). *Arch. Biochem. Biophys.* **267**, 217–227.
Feinleib, S. & Bovey, F. A. (1968). *Chem. Commun.* pp. 978–979.
Fukazawa, T. & Fujita, Y. (1996). *Rev. Sci. Instrum.* **67**, 1951–1955.
Gekko, K. & Matsuo, K. (2006). *Chirality*, **18**, 329–334.
Gekko, K., Yonehara, R., Sakurada, Y. & Matsuo, K. (2005). *J. Electron Spectrosc. Relat. Phenom.* **144–147**, 295–297.
Grossmann, J. G., Hall, J. F., Kanbi, L. D. & Hasnain, S. S. (2002). *Biochemistry*, **41**, 3613–3619.
Hennessey, J., Manavalan, P., Johnson, W., Malencik, D. A., Anderson, S. R, Schimerlik, M. I. & Shalitin, Y. (1987). *Biopolymers*, **26**, 561–571.
Johnson, W. C. (1996). *Circular Dichroism and the Conformational Analysis of Biomolecules*, edited by G. Fasman, pp. 635–652. New York: Plenum Press.
Johnson, W. C. (1971). *Rev. Sci. Instrum.* **42**, 1283–1286.
Kemp, J. C. (1969). *J. Opt. Soc. Am.* **59**, 950–954.
Khazimullin, M. V. & Lebedev, Yu. A. (2010). *Rev. Sci. Instrum.* **81**, 043110.
Majava, V., Löytynoja, N., Chen, W.-Q., Lubec, G. & Kursula, P. (2008). *FEBS J.* **275**, 4583–4596.
Matsuo, K., Namatame, H., Taniguchi, M. & Gekko, K. (2009). *Biosci. Biotechnol. Biochem.* **73**, 557–561.
Matsuo, K., Yonehara, R. & Gekko, K. (2004). *J. Biochem.* **135**, 405–411.
Miles, A. J., Drechsler, A., Kristan, K., Anderluh, G., Norton, R. S., Wallace, B. A. & Separovic, F. (2008*a*). *Biochim. Biophys. Acta*, **1778**, 2091–2096.
Miles, A. J., Janes, R. W., Brown, A., Clarke, D. T., Sutherland, J. C., Tao, Y., Wallace, B. A. & Hoffmann, S. V. (2008*b*). *J. Synchrotron Rad.* **15**, 420–422.
Miles, A. J., Wien, F., Lees, J. G., Rodger, A., Janes, R. W. & Wallace, B. A. (2003). *Spectroscopy*, **17**, 653–661.
Miles, A. J., Wien, F. & Wallace, B. A. (2004). *Anal. Biochem.* **335**, 338–339.
Pysh, E. S. (1976). *Annu. Rev. Biophys. Bioeng.* **5**, 63–75.
Schnepp, O., Allen, S. & Pearson, E. F. (1970). *Rev. Sci. Instrum.* **41**, 1136–1141.
Snyder, P. A. & Rowe, E. M. (1980). *Nucl. Instrum. Methods*, **172**, 345–349.
Stanley, W. A., Sokolova, A., Brown, A., Clarke, D. T., Wilmanns, M. & Svergun, D. I. (2004). *J. Synchrotron Rad.* **11**, 490–496.
Toumadje, A. & Johnson, W. C. Jr (1995). *J. Am. Chem. Soc.* **117**, 7023–7024.
Tseng, P. C., Hsieh, T. F., Song, Y. F., Lee, K. D., Chung, S. C., Chen, C. I., Lin, H. F., Dann, T. E., Huang, L. R., Chen, C. C., Chuang, J. M., Tsang, K. L. & Chang, C. N. (1995). *Rev. Sci. Instrum.* **66**, 1815–1817.

Wallace, B. A. (2000). *Nat. Struct. Biol.* **7**, 708–709.
Wallace, B. A. & Janes, R. W. (2001). *Curr. Opin. Chem. Biol.* **5**, 567–571.
Wallace, B. A. & Janes, R. W. (2003). *Biochem. Soc. Trans.* **31**, 631–633.
Wallace, B. A. & Janes, R. W. (2009). *Modern Techniques for Circular Dichroism and Synchrotron Radiation Circular Dichroism Spectroscopy*. Amsterdam: IOS Press.
Wallace, B. A., Wien, F., Miles, A. J., Lees, J. G., Hoffman, S. V., Evans, P., Wistow, G. J. & Slingsby, C. (2004). *Faraday Discuss.* **126**, 237–243.
Watkins, J., Campbell, G. R., Halimi, H. & Loret, E. P. (2008). *Retrovirology*, **5**, 83.
Whitmore, L. & Wallace, B. A. (2008). *Biopolymers*, **89**, 392–400.
Wien, F., Miles, A. J., Lees, J. G., Vrønning Hoffmann, S. & Wallace, B. A. (2005). *J. Synchrotron Rad.* **12**, 517–523.